

# UAV remote sensing phenotyping of wheat collection for response to water stress and yield prediction using machine learning<sup>☆</sup>



Vikas Sharma <sup>a,b</sup>, Eija Honkavaara <sup>c</sup>, Matthew Hayden <sup>b,d</sup>, Surya Kant <sup>a,b,d,e,\*</sup>

<sup>a</sup> Agriculture Victoria, Grains Innovation Park, 110 Natimuk Rd, Horsham, VIC, 3400, Australia

<sup>b</sup> School of Applied Systems Biology, La Trobe University, Bundoora, VIC, 3083, Australia

<sup>c</sup> Finnish Geospatial Research Institute, National Land Survey of Finland, 02150, Espoo, Finland

<sup>d</sup> Agriculture Victoria, AgriBio, Centre for AgriBioscience, 5 Ring Road, Bundoora, VIC, 3083, Australia

<sup>e</sup> School of Agriculture, Food and Ecosystem Sciences, The University of Melbourne, Parkville, VIC, 3010, Australia

## ARTICLE INFO

### Keywords:

High-throughput crop phenotyping

Yield prediction

Machine learning

Multispectral

UAV

Water stress

## ABSTRACT

Water stress is a significant challenge for global food production. Rainfall pattern is becoming unpredictable due to climate change that causes unprecedent water stress conditions in cereals production including wheat which is one of the important staple food crops. To sustain wheat production under water limiting conditions, there is an urgent need to develop drought-tolerant wheat varieties. For this, screening large numbers of wheat genotype for traits related to growth and yield under water stressed conditions is crucial. In this study, we deployed high-throughput phenotyping approaches, including uncrewed aerial vehicle (UAV)-based multispectral imaging, advanced machine and deep learning regression models. Two separate field experiments, irrigated and rainfed, were conducted comprising 553 wheat genotypes, and collected dataset for traits such as plant height, phenology, grain yield, and timeseries multispectral imaging. UAV-multispectral imagery derived plant height measurements showed a high correlation ( $R^2=0.75$ ) with manual measurements. Vegetation indices derived from multispectral data differentiated growth pattern of genotypes under rainfed and irrigated conditions and were used in yield prediction modeling. Wheat genotypes were effectively ranked, and their response differentiated for water stress tolerance based on yield index, stress susceptibility index, and yield loss%. Importantly, yield prediction in genotypes was computed using four machine learning regression algorithms i.e., linear regression, support vector machine, random forest, and deep learning H2O-3, where H2O-3 was the most accurate model with  $R^2=0.80$ . Results show that multispectral-driven traits combined with machine learning models effectively phenotyped large wheat population and such approaches can be integrated in crop breeding program to develop varieties tolerant to water stress.

## 1. Introduction

Water scarcity is a significant environmental concern, leading to substantial reductions in food production, worldwide. Prediction is that water scarcity will worsen due to increased emissions, contributing to global warming and climate change, particularly in arid and semiarid regions (Liu et al., 2022). By 2050, it is projected that water scarcity will impact more than 50% of global croplands, resulting in crop production to be significantly below the required levels to meet the surging food demand (Alotaibi et al., 2023; Tang, 2020).

Among the major crops grown worldwide, wheat (*Triticum aestivum* L.) is one of the most important staple foods, providing around 20% of

the total calories and protein consumed by humans (Shiferaw et al., 2013). The demand for wheat is projected to rise by 60% by 2050 (Akram et al., 2021). However, wheat production is highly dependent on water availability and is often limited by water stress, particularly in regions with low and variable rainfall (Salem et al., 2022). Insufficient water hampers plant growth and reduces yield by generating reactive oxygen species, stomatal closure, decreased leaf pigments, decline in photosynthesis rate and accelerated plant senescence (Li et al., 2017; Yan et al., 2016). Previous studies have indicated that in the wheat growing cycle, the flowering and grain-filling stages are highly sensitive to water deficit stress. Concurrent water stress at these stages leads to significant reductions in various plant traits, including plant height,

<sup>☆</sup> This article is part of a special issue entitled: "Omics-assisted crop improvement under abiotic stress conditions" published at the journal *Plant Stress*.

\* Corresponding author.

E-mail address: [surya.kant@agriculture.vic.gov.au](mailto:surya.kant@agriculture.vic.gov.au) (S. Kant).

tiller number, leaf area, chlorophyll content, several metabolic processes, and relative water content, resulting in yield losses of more than 50% (Hafez et al., 2020; Ihsan et al., 2016; Muhammad et al., 2022; Zarea and Karimi, 2023). Therefore, developing new wheat varieties with improved water stress resilience is imperative to address the increasing demand for wheat production and the challenges posed by water stress (Bapela et al., 2022).

Plant breeding for developing new wheat varieties require selection of desired traits that confer water stress tolerance. This is achieved through systematic and controlled crossbreeding of different wheat genotypes to create new genetic combinations with the potential to exhibit improved water stress resilience. The breeding process requires meticulous evaluation of numerous progeny lines to identify those that exhibit the desired traits under water stressed conditions. Researchers have investigated the potential of traditional methods for improving water stress resilience in wheat through the selection of genotypes with desirable physiological traits. For example, measurements of transpiration, stomatal conductance, photosynthesis, shoot biomass, and grain yield were taken in wheat genotypes to screen for response to water (Alotaibi et al., 2023; Bapela et al., 2022; Dang et al., 2021; Gavuzzi et al., 1997; Hafez et al., 2020; Ihsan et al., 2016; Wilke et al., 2021). Certainly, these studies provide important insights into the physiological mechanisms underlying water stress resilience in wheat and the potential for selecting genotype with improved performance. However, these traditional phenotyping methods are laborious, time-consuming, destructive, subjective, and may not be scalable for screening larger populations (Koh et al., 2021; Thoday-Kennedy et al., 2023).

To overcome these challenges and to match the genomics advancement in order to accelerate the development of new wheat varieties tolerant to water stress, there is a need of high-throughput crop phenotyping (HTCP) methods which can provide the near real-time data in non-destructive way for larger field experiments. To this end, remote sensing (RS) opens the way with its variety of data i.e., color, multispectral, hyperspectral with various platforms such as airborne and spaceborne, for timely detection of various plant traits in high temporal resolution. RS captures spectral readings by measuring the interaction between incoming radiation and target objects, creating unique signatures of reflected light. Multispectral satellite-based RS is successfully being used for HTCP for larger (Pinto et al., 2023; Sankaran et al., 2015; Tattaris et al., 2016; Thoday-Kennedy et al., 2023). However, satellite datasets could be of lower spatial and spectral resolution, limited temporal revisit, atmospheric interference, and cost constraints can hinder its effectiveness for HTCP, especially when a large population have been sown in the small plots or in a single line fashion (Choudhury et al., 2019).

To surmount these obstacles, uncrewed aerial vehicle (UAV) mounted with low-cost multispectral sensors are suitable options as they can offer thematic information at ultra-spatial resolution in comparison of satellites (Goswami et al., 2019). Several vegetation indices (VIs) can be derived from this data which can be used further to correlate with ground data in order to estimate the plant traits and to predict the yield (Dang et al., 2021; Joshi et al., 2023; Naghdyzadegan et al., 2023; Panda et al., 2010; Qiao et al., 2021). A number of studies used these VIs to detect the abiotic stress (Mwinuka et al., 2022), biotic stress (Su et al., 2018) and to estimate various plant traits i.e., emergence count (Sankaran et al., 2015), plant density (Wilke et al., 2021), height (Xie et al., 2021), biomass (Sankaran et al., 2018), canopy cover, leaf area index (Córcoles et al., 2013), chlorophyll (Qiao et al., 2022), nitrogen (Liao et al., 2023), protein (Wolters et al., 2022), and yield prediction (Zhou et al., 2021a). Among all, yield prediction stands out as a crucial trait since it enables timely and accurate evaluation of grain yield before harvest, facilitating the selection of elite genotypes in large breeding programs (Panda et al., 2010). An array of methodologies, spanning from process-based models elucidating physiological mechanisms to data-driven statistical algorithms, has been formulated and employed for crop yield prediction.

Nonetheless, due to the limitations imposed by timeseries data unavailability for parameterization, model calibration, and validation of process-based models, statistical techniques present promising alternatives and supplementary tools (Naghdyzadegan et al., 2023; Ruan et al., 2022; Srivastava et al., 2022). Furthermore, conventional prediction methods are incapable of effectively managing large volumes of complex time-series data and often suffer from overfitting (Cheng et al., 2022; Joshi et al., 2023). To this end, machine learning (ML) and deep learning (DL) algorithms emerge as favorable choices, owing to their adeptness in managing substantial datasets and providing a range of hyperparameter tuning options (Chouhan et al., 2022). Established ML methods such as random forest (RF) (Breiman, 2001; Ruan et al., 2022), support vector machine (SVM) (Cortes and Vapnik, 1995; Dang et al., 2021) and DL (Arno Candel, 2020; LeCun et al., 2015; Qiao et al., 2021) have been used to build yield forecasting models which uses the timeseries RS data with ground measurements to achieve higher prediction accuracy (Dang et al., 2021), decreased time complexity (Qiao et al., 2021), and sustained reliability (Goswami et al., 2019; Sharma et al., 2016).

A few studies have demonstrated the use of RS for the screening of wheat genotypes for water stress and highlight the advantages of this approach over traditional methods (Bapela et al., 2022; Li et al., 2017; Mwinuka et al., 2022). However, most of these studies have focused on a limited number of wheat genotypes and only on few timepoints of data instead of continuous timeseries. Therefore, this research focuses on the assessment of the high-throughput UAV multispectral imaging and advanced regression methods supported by ground measurements to screen 553 wheat genotypes for water stress with the following objectives; (i) phenotype wheat collection based on the yield, phenology and time series VIs, (ii) compare the performance of different ML algorithms and to identify the most accurate model for predicting wheat yield, and (iii) identify wheat genotypes that exhibit higher growth and yield in water stress based on yield index.

## 2. Material and methods

### 2.1. Field experiment details

The experiment was conducted at SmartFarm, Agriculture Victoria, Horsham, Victoria, Australia in 2019 (Fig. 1). Horsham is located in the temperate climate and medium rainfall zone, with an average annual rainfall of 370 mm. The experiments were conducted as rainfed (RaF) with natural rainfall and irrigated (IRR) with application of 125 mm irrigation. The sowing and harvesting for field experiments were done on 31st May 2019 and in the third week of December 2019, respectively. The experiments were a complete block randomized design with 553 wheat genotypes and three replications which counts 1659 wheat crop plots for each experiment. Experimental plots were of dimension 5 × 1 m. Genotypes used in this study were single seed descent and were assigned unique codes, details provided in Supplementary Table 1.

Manual measurements were collected in the experiment area, including plant height, days to heading (DTH), days to maturity (DTM), 1000 grain weight (1000GW) and grain yield. Plant height was measured from all plots in both experiments at near physiological maturity where five representative plants were selected in each plot and measured from ground level to the tip of spike (excluding awns). The DTH was recorded as number of days from sowing to when 50% plants in the plot were heading. The DTM was recorded as the number of days from sowing to when 90% of the plants in plot reached physiological maturity. Days of grain filling (DoG) were calculated as difference of DTM and DTH. Grain yield was collected from each individual plot after machine harvest.

### 2.2. Weather and irrigation during experiment cycle

Weather information was acquired using field-based weather station (MEA Pty. Ltd., Adelaide, Australia), positioned at the experimental

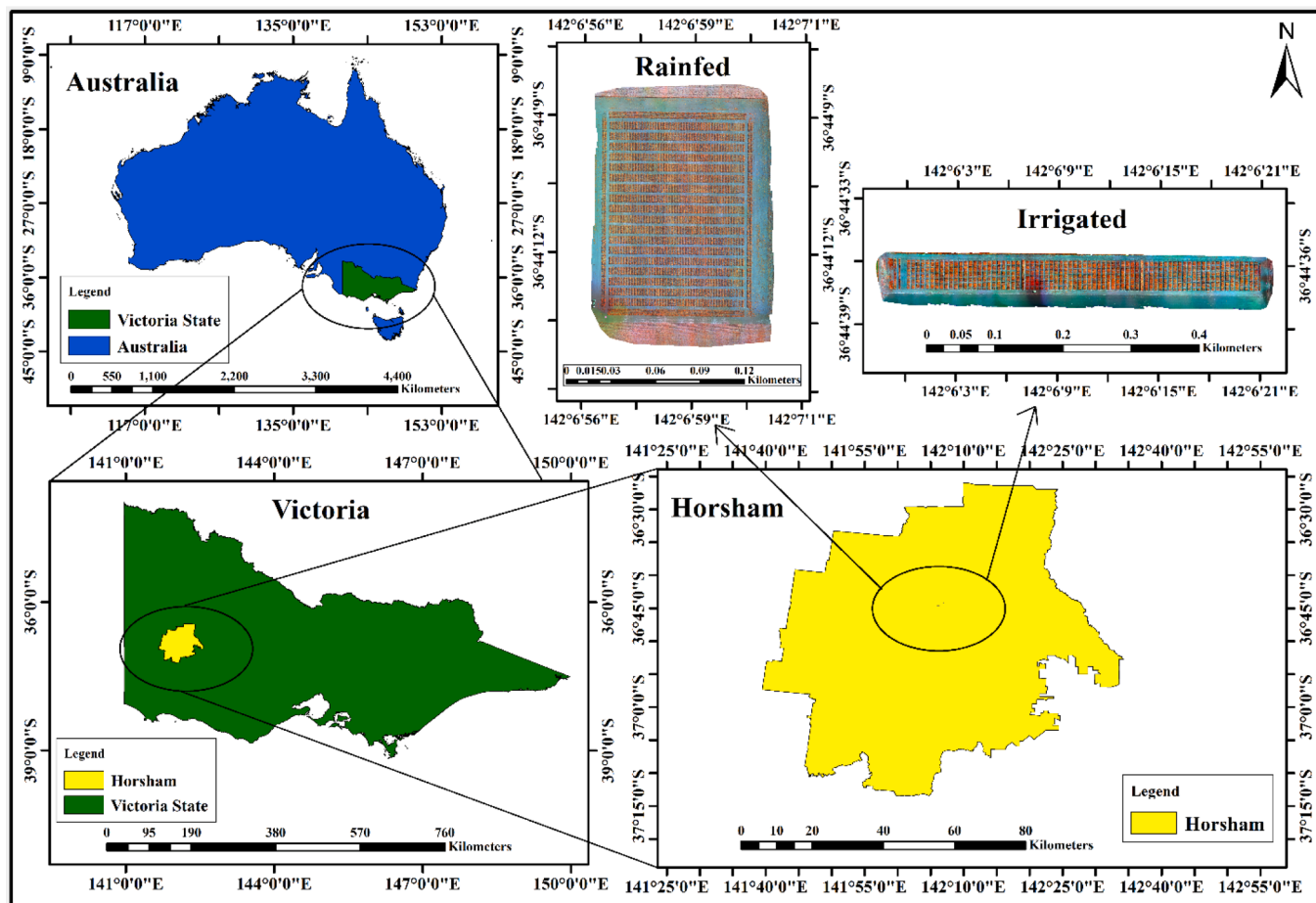


**Fig. 1.** Map showing the location of irrigated and rainfed field experiments.

sites. The experimental sites received below average rainfall, with a total 290 mm for whole year, out of this 219.8 mm of rainfall was recorded during the crop growth cycle (Fig. 2). In the IRR experiment, irrigation was supplied twice i.e., prior to sowing and during the grain filling stage, applying 75 mm and 50 mm of irrigation, respectively.

### 2.3. Aerial data collection and processing

A time series of multispectral UAV data was gathered on cloud free days, commencing from 60 days after sowing (DAS) until 192 DAS, with a temporal interval of ~15 days, resulting in a total of 10 timepoints.

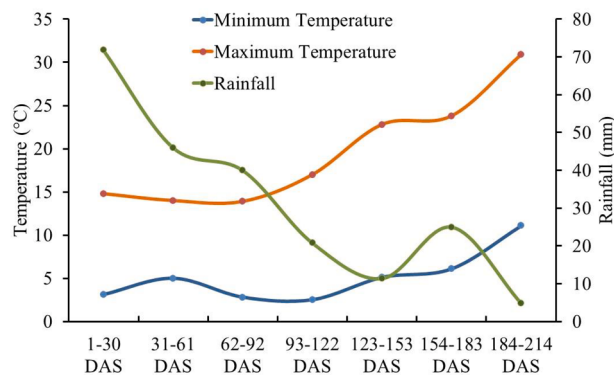


**Fig. 2.** Weather data for crop growth season. Minimum average temperature, maximum average temperature, and total rainfall are shown at different days after sowing (DAS).

Date of flights with respective DAS is presented in Supplementary Table 2. To collect this data, a DJI Matrice 100 quadcopter (DJI, Shenzhen, China) equipped with a MicaSense RedEdge multispectral camera (MicaSense Inc., Seattle, USA) were employed (Fig. 3). Prior to flight, the imaging system was configured to capture images automatically at a height of 35 m, achieving a ground sampling distance of 2.43 cm. The image acquisition process was triggered by the GPS module, which operated in an automated capture mode, with acquisition set to 85% forward and side overlap. The MicaSense RedEdge multispectral camera, which collects energy in five spectral bands, including blue (475 nm), green (560 nm), red (668 nm), red edge (717 nm), and near-infrared (840 nm), was calibrated with pre-calibrated reflectance panel and its known coefficients for individual multispectral bands (blue-0.4893, green-0.4895, red-0.4899, red edge - 0.4901 and NIR - 0.4905) to reduce radiometric effects (Fig. 3c). Radiometric calibration measurements were systematically acquired by the multispectral sensor preceding each flight mission, serving as a prerequisite for precise image correction. To achieve geometric precision at the centimeter level, the data collection process involved installing five ground control points (GCPs) in each field, with one at the center and the remaining four at the corners. The positions of these GCPs were measured using a multi-band global navigation satellite system (GNSS) based on real-time kinematic (RTK) positioning receiver (Reach RS2, Emlid Ltd., Hong Kong) which gives the accuracy of 0.02 m in planimetry and 0.03 m in altimetry (Banerjee et al., 2021; 2020).

At each flight time point, a substantial number of images (~3500 for each field experiment) were captured, necessitating rigorous radiometric and geometric processing followed by mosaicking to produce each individual orthomosaic band. This process was done using Pix4D

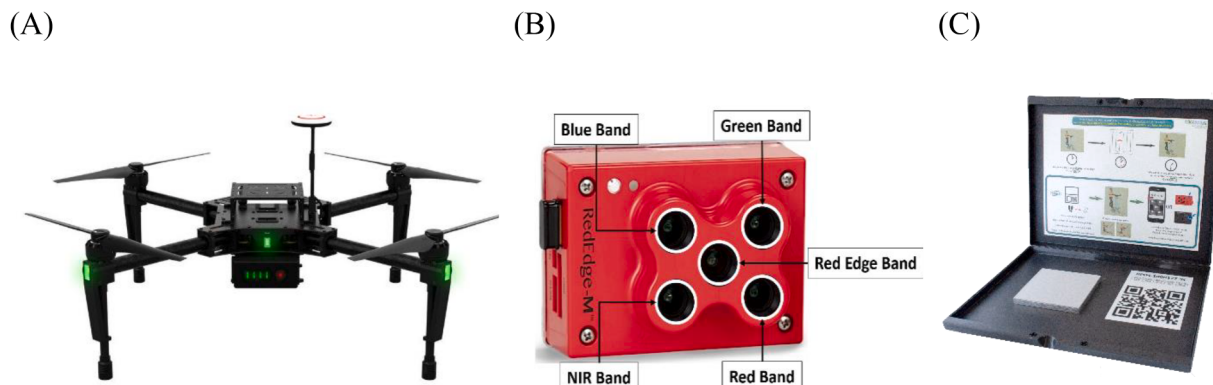


**Fig.. 3.** UAV system used for data collection. (A) DJI Matrice 100 quadcopter, (B) Five band multispectral camera, and (C) Calibration panel.

Mapper software (Pix4D SA, Lausanne, Switzerland) which utilizes structure from motion algorithm for image georeferencing and point cloud generation. Furthermore, locations of five GCPs collected from each experiment were inputted in this software, to ensure geometric accuracy of orthomosaic. The generated bands were referenced in the Universal Transverse Mercator (UTM) coordinate system with World Geodetic System 1984 (WGS84) as the geodetic datum. Utilizing a digital elevation model (DEM) derived from the point cloud, the multiple images were stitched in order to produce an orthomosaic. The conversion of raw radiance into surface reflectance was achieved using a downwelling light sensor, which effectively accounted for variations in irradiation throughout the data acquisition process (Aasen et al., 2018). After generating the orthomosaic data, a shapefile was created in QGIS (<http://www.qgis.org>) to extract the plot level trait summary and reduce the edge effect.

#### 2.4. Vegetation and yield based water stress indices

Important UAV based VIs such as normalized difference vegetation index (NDVI), normalized difference red edge (NDRE), canopy chlorophyll content index (CCCI), and crop volume (CV) were computed as described in Table 1. The selection of these VIs was based on their ability to provide significant information about plant health in water limited conditions. NDVI and NDRE are the most used VIs in RS, where NDVI being sensitive to changes in vegetation coverage and NDRE leverages the reflectance values in the red edge region of the electromagnetic spectrum, which is sensitive to variations in chlorophyll content and overall plant vitality. The CCCI index estimates chlorophyll level in the plant canopy. The CV was computed to obtain information of biomass. On the other hand, digital terrain model data was subtracted from digital surface model data to get the UAV derived height of plants. For each plot, all the VIs were calculated by taking the average of all pixel values

**Table. 1**  
Vegetation and yield indices used in this study.

Index	Equation	Reference
NDVI	NIR – RED/NIR + RED	(Rouse J, 1973)
NDRE	NIR – RE/NIR + RE	(Clarke et al., 2001)
CCCI	(NDRE – NDREmin)/(NDREmax – NDREmin)	(Perry et al., 2012)
CV	Crop height X Crop coverage	(Banerjee et al., 2020)
Yield index	Yield in Stress/Yield in Control	(Gavuzzi et al., 1997)
Stress susceptibility index	Yield in Stress X Yield in Control / Yield in Control <sup>2</sup>	(Rosielie & Hamblin, 1981)
Yield loss%	(1 – Yield in Stress/Yield in Control) × 100	(Pimentel et al., 2015)

in the plot.

In conjunction with these UAV multispectral VIs and manual data-based yield indices i.e. yield index, stress susceptibility index (SSI), and yield loss% were also calculated to assess the yield potential of each genotype in water stress conditions. A high value of yield index shows high water stress tolerance capacity, whereas a high yield loss% suggests lower water stress tolerance of genotype. On the other hand, the lower value of SSI indicates that the genotype was tolerant and vice versa. The equations of all indices are presented in Table 1.

#### 2.5. Yield prediction using deep and machine learning regression algorithms

To ensure a comprehensive evaluation of the predictive models, different ML algorithms were used, each chosen from distinct categories of the statistical analysis. The inclusion of these diverse algorithms ensured a comprehensive comparison of different ML methods in the prediction of crop yield.

##### 2.5.1. Linear regression

Linear regression, a parametric algorithm, was chosen to represent the class of linear models. Linear regression models the relationship between a dependent variable and one or more independent variables. The algorithm fits a linear equation to find the line of best fit that minimizes the difference between the predicted values and the actual values. The equation takes the form of  $Y = a + bX$  where Y is the dependent variable, X is the independent variable, a is the intercept, and b is the slope of the line (Schneider et al., 2010).

##### 2.5.2. Support vector machine (SVM)

SVM was selected from non-parametric category, which can effectively capture non-linear relationships between variables. SVM regression tries to find the best hyperplane that can predict the output variable for new input data. SVM uses different types of kernel functions such as linear, polynomial, radial basis function (RBF), and sigmoid, to transform the data into a higher dimensional space to improve the accuracy and reduce the time complexity of the model (Cortes and Vapnik, 1995; Dang et al., 2021; Sharma et al., 2016).

##### 2.5.3. Random forest (RF)

RF was selected to represent the category of ensemble algorithms, which leverage decision trees for prediction. Each decision tree is constructed using a random subset of the training data and a random subset of the input features. This helps to reduce overfitting and improve the accuracy of the model. During the prediction phase, the RF takes the average of all the predictions from each individual tree to produce the final prediction (Breiman, 2001; Chutia et al., 2017).

#### 2.5.4. Deep learning (DL)

A DL model H2O-3 was used, which is based on artificial neural networks and can efficiently handle high-dimensional data. H2O-3 is based on recurrent neural networks, which are composed of interconnected layers of neurons that use activation functions such as hyperbolic tangent (tanh), rectified linear unit (ReLU), and maxout. This algorithm uses backpropagation technique for training and adjusts the weights and biases of the neurons in the network to minimize the difference between the predicted output and the actual output. The optimization process is typically carried out using stochastic gradient descent or one of its variants, which involves computing the gradients of the loss function with respect to the model parameters and updating the parameters in the direction of the negative gradient. To improve predictive accuracy, this model incorporates advanced features like adaptive learning rate, momentum training, rate annealing, dropout, L1 or L2 regularization, checkpointing, and grid search (Arno Candel, 2020; Cheng et al., 2022; LeCun et al., 2015).

#### 2.5.5. Supervised training of the models

To predict the yield, timeseries (all 10 timepoints) NDVI, CCCI, NDRE, CV, 5 multispectral bands with DTM were used as input features. This data was randomly split into training (67%) and testing (33%). To estimate the accuracy of the models and mitigate overfitting, a 10-fold cross-validation approach was employed, which involves dividing the data into 10 equally sized subsets, training the model on 9 subsets, and evaluating its performance on the remaining subset. The performance of each regression algorithm was assessed using root mean square error (RMSE), normalized root mean square error (NRMSE) and coefficient of determination ( $R^2$ ).

#### 2.6. Statistical analysis

A t-test analysis was conducted to determine significant differences between RaF and IRR experiments on various plant traits such as phenology, plant height, yield, and 1000GW. The resulting p-value indicated the strength of statistical significance. Furthermore, a Pearson correlation test was used to assess the correlation between plant height measurements obtained from UAV and manual measurements.

### 3. Results

#### 3.1. Plant growth and phenology between irrigated (IRR) and rainfed (RaF) experiments

A significant difference was recorded for DoG, plant height, and grain yield between RaF and IRR experiments (Fig. 4). For DoG, the RaF experiment displayed a median of approximately 36 days, slightly shorter than the IRR experiment's median of about 45 days (Fig. 4A). For plant height, the IRR experiment had taller plants than RaF. The median height for the RaF experiment was 86 cm, while the IRR experiment had 105 cm (Fig. 4B). The average yield in IRR experiment was significantly higher (1612 g) than the RaF (860 g) (Fig. 4C). The comparison of 1000 grain weight between IRR and RaF experiments showed no difference, (Fig. 4D).

##### 3.1.1. Genotype ranking

Genotype ranking was performed based on the yield index, SSI, and yield loss%, these indices are capable in identifying genotypes that perform well under control and water stress conditions (Joshi et al., 2021). Genotype ranking based on these indices for all 553 genotypes is provided in Supplementary Table 1. Five top performing (green bars), five medium performing (blue bars), and five least performing (red bars)

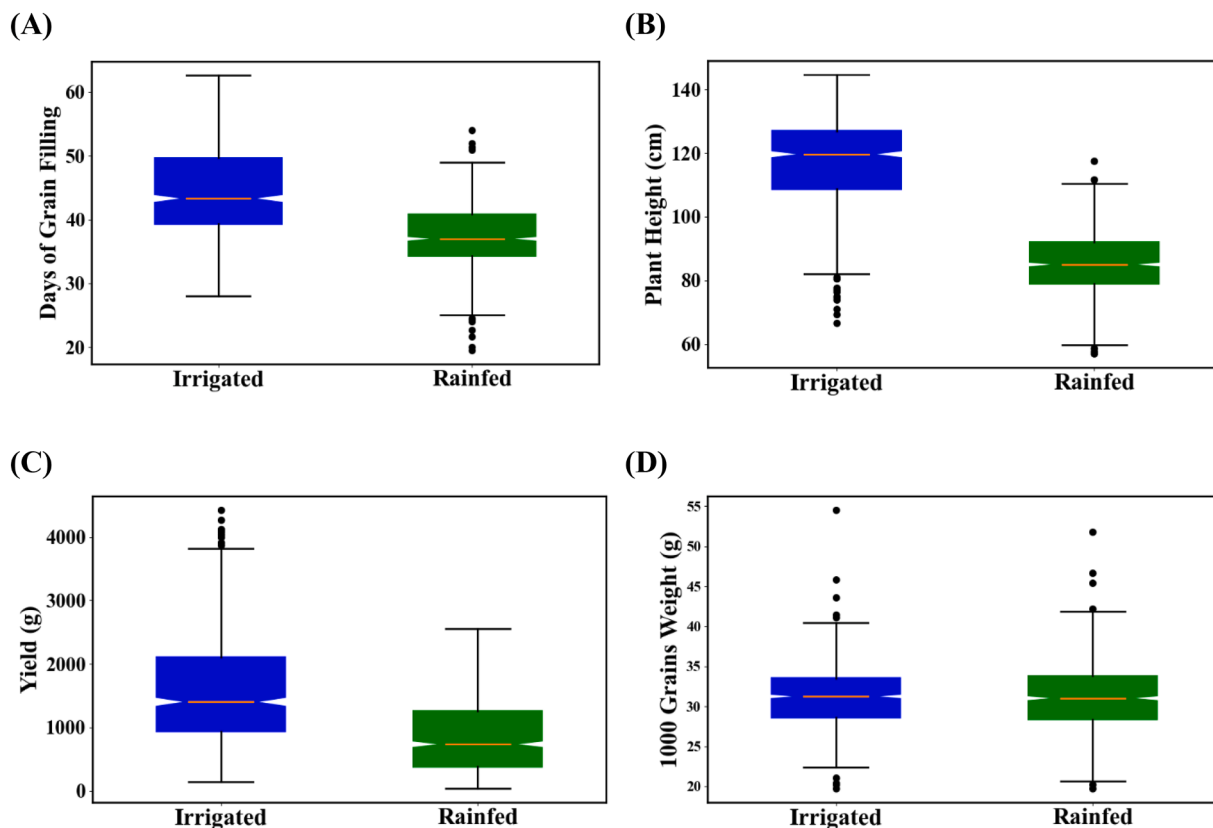


**Fig. 4.** Distribution of phenology, plant height and yield of rainfed and irrigated experiments. (A) days of grain filling, (B) plant height, (C) yield, and (D) 1000 grain weight. Blue bar shows the irrigated field, green bar shows the rainfed field and orange line inside the boxplots shows the median of data.

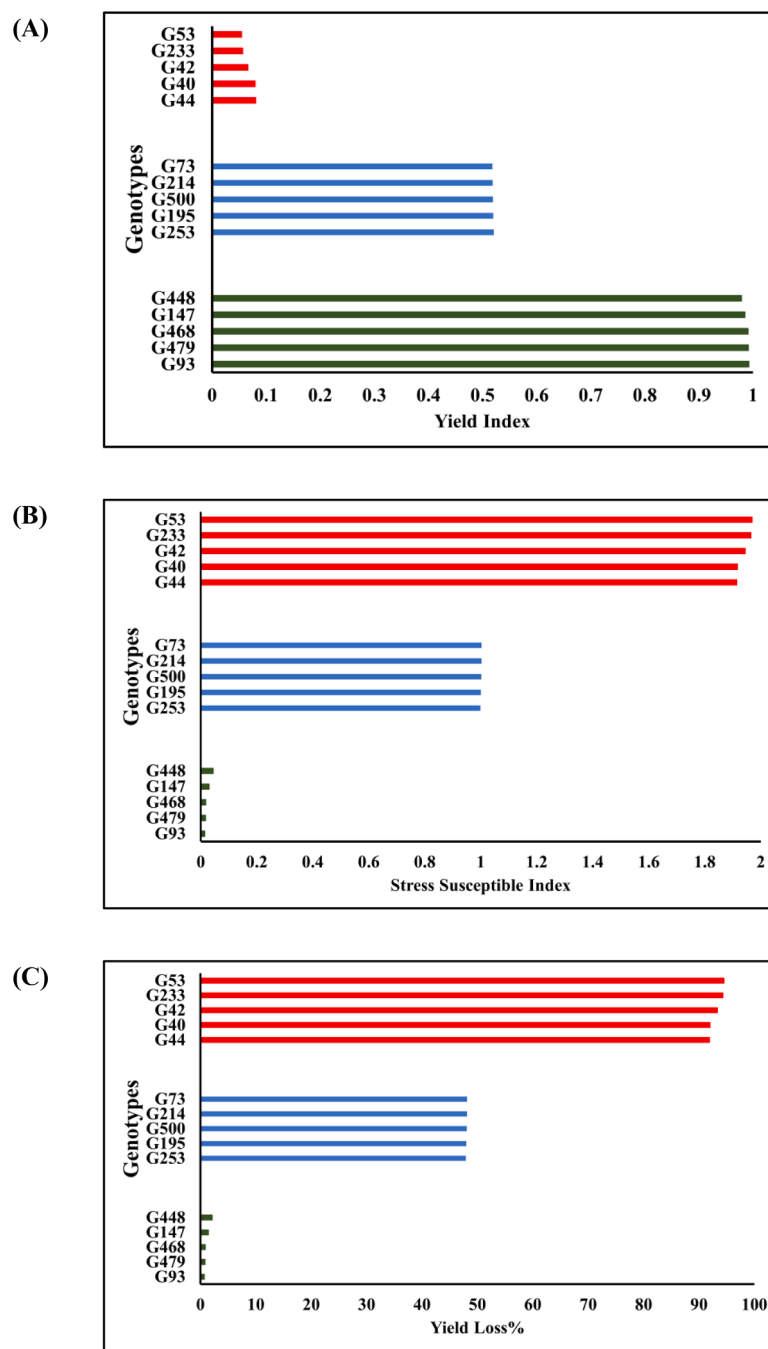


**Fig. 5.** Genotype ranking for water stress condition. (A) yield index, (B) stress susceptibility index, and (C) yield loss%. Five top performing (green bars), five medium performing (blue bars), and five least performing (red bars) genotypes are shown.

genotypes are shown in Fig. 5, providing a representative overview of the range of these indices value observed in the wheat genotypes. The analysis revealed that genotypes G93, G479, G468, G147, and G448 had the highest yield index values (~0.99), lowest SSI value (~0.02) with yield loss% (~1%). Whereas genotypes G253, G195, G500, G214, and G73 had moderate values of yield index (~0.52), SSI (~1), and yield loss % (~48%). On the other hand, genotypes G44, G40, G42, G233, and G53 exhibited low yield index values (~0.06), high SSI value (~1.95) with yield loss% (~93%).

### 3.2. Vegetation indices (VIs) differentiated growth pattern under irrigated and rainfed experiments

The NDVI and NDRE values were consistently higher in IRR experiment than RaF except at 60 DAS (dark orange bars) and 90 DAS (gray bars) (Fig. 6A and B). The average maximum values of both VIs were recorded at 136 DAS (dark green bars) (NDVI; IRR = 0.95, RaF = 0.85, and NDRE; IRR = 0.65 and RaF = 0.55). On the other hand, CCCI values were higher in IRR in comparison of RaF from beginning till 163 DAS (light sky-blue bars) (Fig. 6C). The highest value of CCCI were recorded at 117 DAS in RaF and 136 DAS (dark green bars) in IRR experiment. The CV result showed a slightly different pattern compared to the other VIs. In the initial stages, up until 90 DAS, the RaF experiment had higher

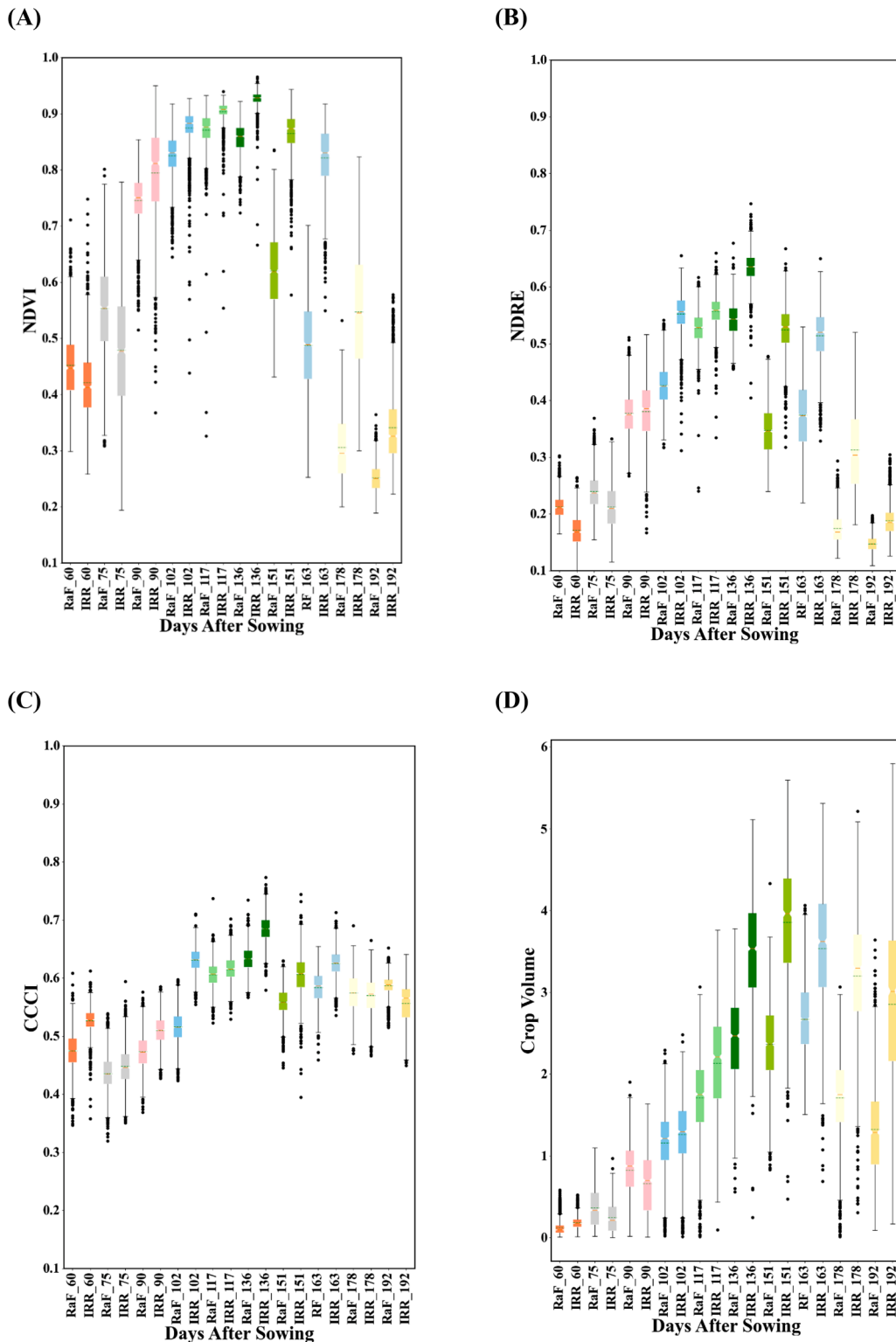


**Fig. 6.** Timeseries UAV derived vegetation indices throughout the crop cycle in rainfed (RaF) and irrigated (IRR) fields. (A) Normalized difference vegetation index (NDVI), (B) Normalized difference red edge (NDRE), (C) Canopy chlorophyll content index (CCCI), and (D) Crop volume (CV). Rainfed and irrigated fields at 60 DAS (orange bars), 75 DAS (gray bars), 90 DAS (light pink bars), 102 DAS (sky blue bars), 117 DAS (light green bars), 136 DAS (dark green bars), 151 DAS (olive green), 163 DAS (light sky-blue bars), 178 DAS (light yellow bars), and 192 DAS (dark yellow bars).

values of CV, but after that, the IRR experiment had consistently higher values of CV (Fig. 6D).

### 3.3. Regression analysis between UAV-derived and manual measurements

The regression assessment between manually measured height and UAV derived height revealed significantly high relationship (Fig. 7). The calculated coefficient of determination ( $R^2=0.75$ ) indicates linear

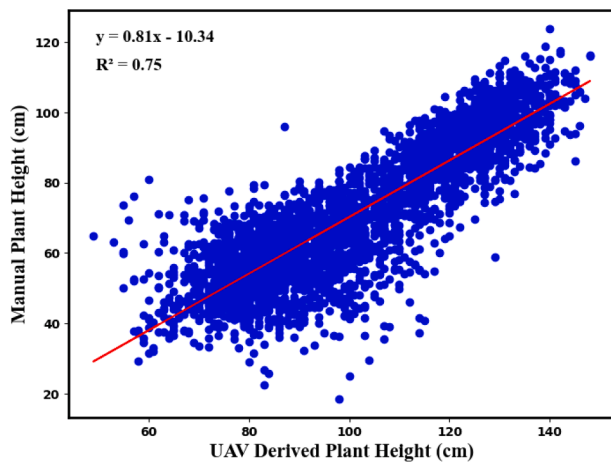


**Fig. 7.** Regression analysis of UAV derived and manually measured plant height.

correspondence between manual and UAV derived plant height measurements.

Another correlation analysis was conducted between manual measurements such as DTM, DoF, 1000GW, and yield, in relation to UAV multispectral derived VIs including NDVI, NDRE, CCCI, and CV at 110 DAS across both experiments. The results were visualized using radar charts and a correlation matrix (Fig. 8).

In the RaF experiment, a higher correlation was found between 1000GW and NDVI ( $R = 0.71$ ), NDRE ( $R = 0.70$ ), and CCCI ( $R = 0.64$ ). Additionally, DTM exhibited positive correlations with NDRE ( $R = 0.63$ ) and CCCI ( $R = 0.67$ ), whereas a negative correlation with CV ( $R = -0.68$ ). Furthermore, CV demonstrated a correlation coefficient of 0.54 with yield (Fig. 8A and B). Conversely, in the IRR experiment, DTM displayed positive correlations with NDVI ( $R = 0.82$ ), NDRE ( $R = 0.63$ ), and CV ( $R = 0.51$ ). Interestingly, DoG exhibited negative correlations with all VIs, with the most substantial negative correlation observed with NDVI ( $R = -0.62$ ) (Fig. 8C and D).

#### 3.4. Modeling for yield prediction

Yield prediction was done using regression analysis, ML and DL algorithms incorporating timeseries UAV derived and ground measurement data. Each model's performance was assessed using  $R^2$ , RMSE and NRMSE. The results presented below are based on the evaluation of the models using test data. For the linear regression model, the  $R^2$  was 0.66, with RMSE of 489.91 and NRMSE of 0.002 g per plot, indicating that approximately 66% of the variance in yield can be explained by this model (Fig. 9A). The non-parametric SVM model demonstrated higher predictive capabilities than linear regression, particularly when initialized with the RBF kernel, where regularization parameter of 1 and gamma function of 0.01 were used. The SVM model exhibited an  $R^2$  of 0.72, an associated RMSE of 454 and NRMSE of 0.126 g per plot (Fig. 9B). Furthermore, RF model was executed with 100 C4.5 decision trees. The RF demonstrated promising performance with an RMSE of 434, NRMSE of 0.149 g per plot and  $R^2$  of 0.74 (Fig. 9C), indicating that the model could predict the actual yield values with reasonable accuracy, slightly higher than both SVM and linear regression. Similarly, DL model H2O-3 was initialized with 64 neurons, ReLU activation function, stochastic gradient descent optimization, 0.001 learning rate, 200 epochs, and L2 regularization. The model achieved an RMSE value of 376, NRMSE of 0.119 g per plot and  $R^2$  of 0.80 (Fig. 9D).

#### 4. Discussion

Water stress continues to threaten global food security, therefore, the

development of drought-resilient varieties in important cereal crop wheat is imperative to ensure sustainable food production (Zhou et al., 2021a). Phenotyping a large population of crop is laborious and difficult task for plant breeders. To record the data on different agronomic traits of genotypes during different stages of growth is challenging through manual measurements. Subtle phenotypic variation among the genotypes is not visible to the human eye and does not reflect in the recorded observation. Manual data collection become unfeasible in situations such as when field is wet due to rainfall or irrigation and water is standing in the experiment. In addition, through visual/manual observation, plant breeder can evaluate a limited number of genotypes, therefore, results remain limited or some time desirable plant may escape or lost due to rejection (Qiao et al., 2022; Wilke et al., 2021). For a plant breeder, evaluation during F2 to F6 generations is a challenging task, it requires more time with full attention during selection and rejection of plants from the large population to identify the most desirable recombinants having desirable traits of both the parents (Tattaris et al., 2016).

By deploying HTCP technologies, this research evaluated a large collection of 553 wheat genotypes under both IRR and RaF field conditions. Wheat yield was predicted using UAV multispectral derived VIs and ground observations analyzed through regression algorithms. The findings of this study underscore the importance of HTCP methods in rapidly advancing genetics for water stress tolerance. The computation of VIs including NDVI, NDRE, CCCI, and CV, offered valuable insights into physical crop traits contributing to a comprehensive assessment of plant performance.

Comparative analysis between RaF and IRR experiments highlighted significant differences in plant growth and yield-related traits. The observed variations in DoG, plant height, and yield evaluated the impact of water availability on wheat growth and development (Xie et al., 2021). The DoG is an important developmental phase in wheat, as it directly impacts the final yield. The longer the grain filling period, the more time the wheat plants have for accumulation and allocation of photosynthates for grain filling, resulting in higher yield (Zarea and Karimi, 2023). The broader range of DoG and taller plants in the IRR experiment suggests that water availability plays a crucial role in determining the duration of the grain filling phase and overall plant growth. The shorter DoG observed in RaF experiment due to limited water availability that led to lower grain yield. The findings suggest that while both experiments experienced some degree of yield variability, the IRR experiment had a more consistent yield distribution and higher yield overall.

The genotype ranking based on the yield index, SSI, and yield loss% provided valuable insights into the performance of different genotypes under water stress conditions. The identification of genotype with high yield index and low SSI and yield loss% values indicate their potential for achieving higher growth and productivity in water limited environments. These results suggest that the top performing genotypes G93, G479, G468, G147, and G448 may possess certain traits that contribute to their higher water stress tolerance and yield potential and may be more suitable for cultivation in areas with limited water availability. This ranking approach holds promise for selecting and breeding genotypes with improved water stress resilience, contributing to the development of drought-tolerant wheat varieties.

In evaluating the efficacy of high-throughput phenotyping as a replacement for manual observations, a high correlation between manual measured and UAV derived plant height ( $R^2=0.75$ ) suggests that digital technology can be used as an alternative to manual observations (Xie et al., 2021). Furthermore, reasonable correlation of VIs with other manual plant traits DTM correlations with NDRE ( $R = 0.63$ ) and CCCI ( $R = 0.67$ ), and CV ( $R = -0.68$ ) at 110 DAS suggests that these indices hold potential for plant assessment in high temporal resolution (Panda et al., 2010). The average maximum values of NDVI and NDRE was observed at 136 DAS which was just before the flowering followed by a decline in the later stages. This trend is expected as the crop approaches maturity.

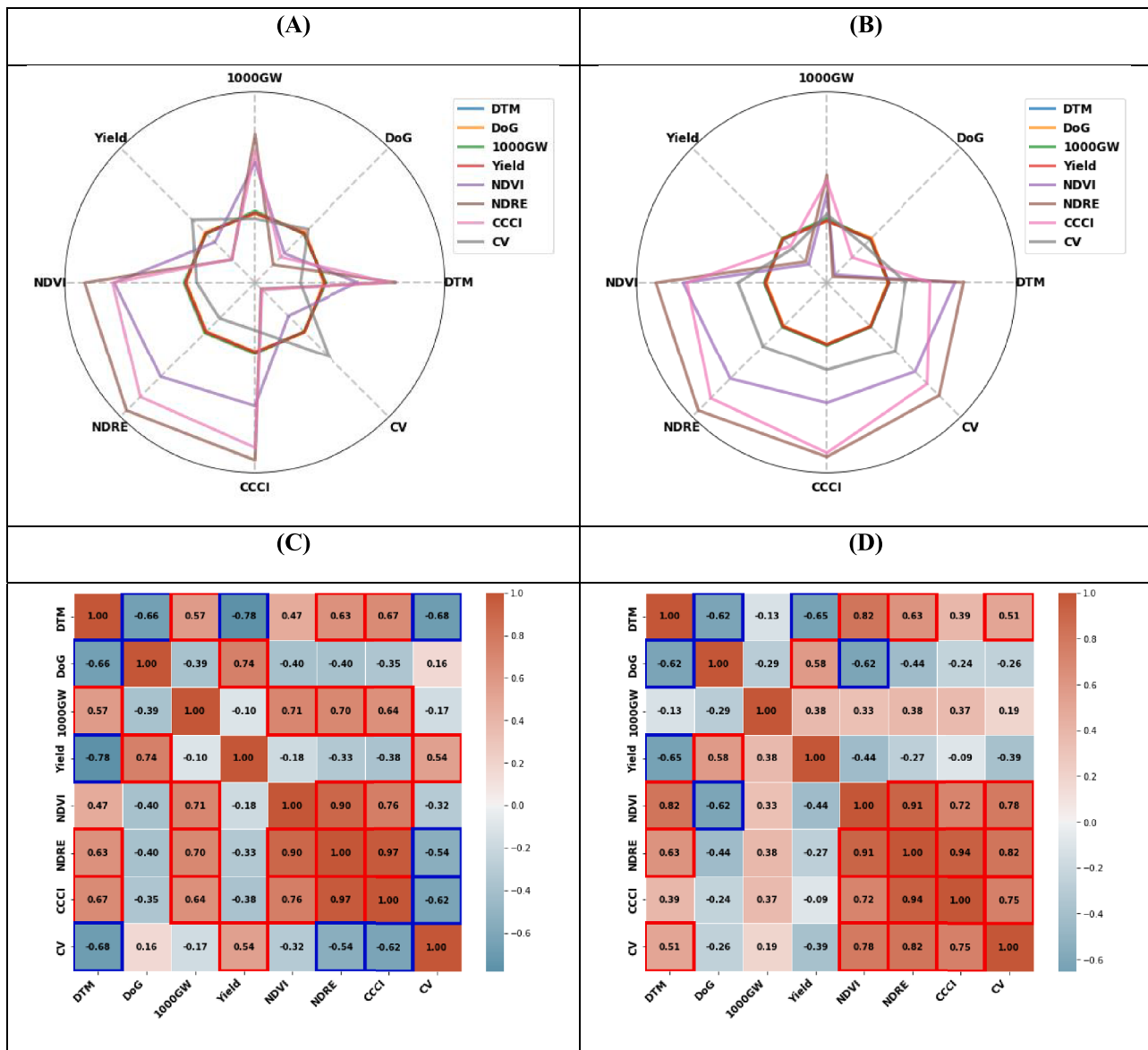


**Fig. 8.** Correlation of UAV multispectral data with manual measurements. (A) radar chart of rainfed (RaF), (B) radarchart of irrigated (IRR), (C) correlation matrix of RaF, and (D) correlation matrix of IRR. Data was collected on 110 days after sowing. Days to maturity (DTM), Days of grain filling (DoG), normalized difference vegetation index (NDVI), normalized difference red edge (NDRE), canopy chlorophyll content index (CCCI), crop volume (CV).

These observations gave important information about crop greenness which can be further related to crop health. On the other hand, the CCCI values did not show much variation between genotypes in both experiments, indicating that the chlorophyll content in the crop canopy was not affected as much by irrigation as it was by the overall biomass (Fig. 6C).

The core of this study relies in the evaluation of various regression algorithms for predicting wheat yield using UAV based multispectral data. Linear regression results suggest a moderate degree of predictability, but there is still considerable unexplained variability in the data which further requires the advance regression methods to manage the variability in data. To this end, the SVM model showed the promising results ( $R^2=0.72$ ), indicating a more pronounced alignment with the data and decreased prediction error compared to the linear regression approach. In addition, ensemble-based RF model also achieved similar predictive accuracy with  $R^2$  of 0.74 but one limitation of the model is that it does not provide direct insight into the underlying relationships between the predictor variables and the target variable. Although the model can identify important features, it does not explicitly provide

information on how these features are related to the target variable. Specifically in situations where the relationships between predictor variables and the target variable are highly complex and non-linear, DL regression algorithms like H2O can be a promising alternative to traditional regression models. This is because DL models are capable of identifying and modeling intricate patterns and relationships in the data, in cases where traditional models may struggle. The results revealed that the DL regression model H2O-3 outperformed the other algorithms in terms of prediction accuracy ( $R^2=0.80$ ), RMSE of 376 and NRMSE of 0.119 g per plot. This finding highlights the potential of DL approach to harness the power of complex neural networks in capturing intricate relationships between input features and output variables.

It is worth noting that the adoption of ML and DL methods for yield prediction leverages the advantages of handling large and complex datasets while providing options for hyperparameter tuning. The success of the DL model H2O-3 suggests its potential as an efficient tool for crop yield prediction, offering a promising avenue for future applications in agricultural research and breeding programs.

The results underscore the potential benefits of UAV multispectral

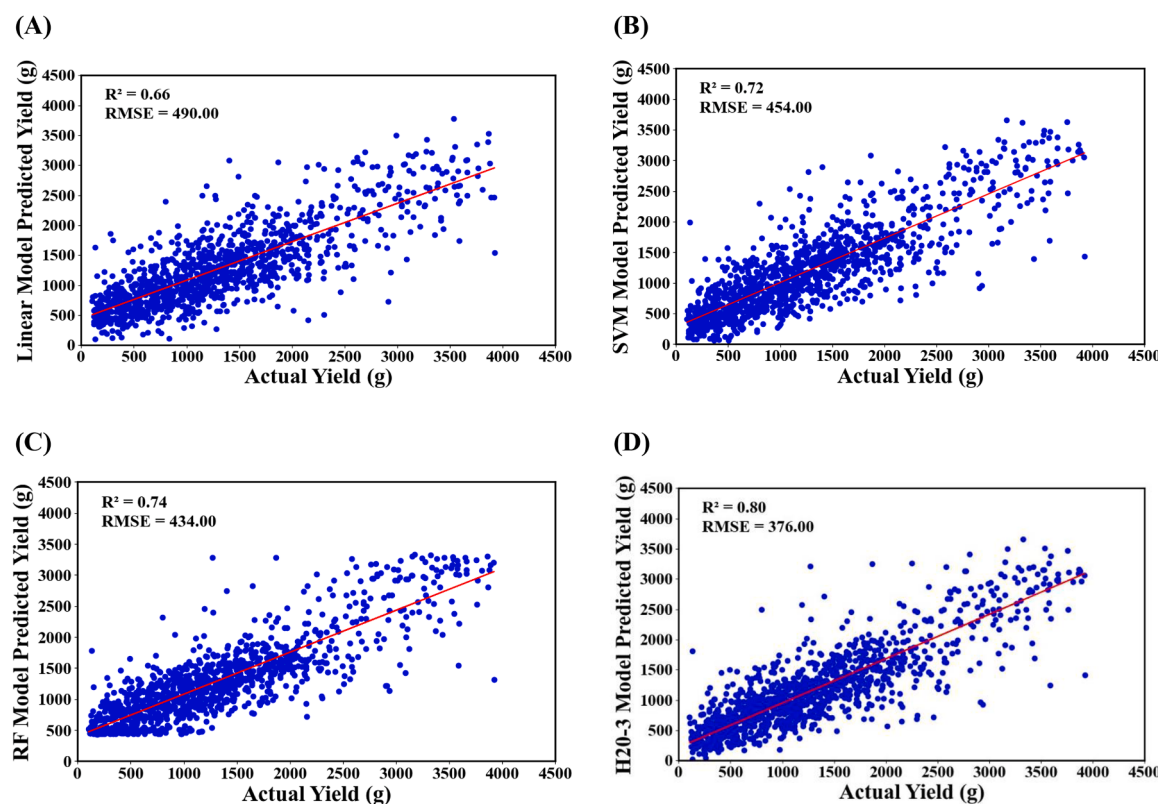


**Fig. 9.** Yield prediction for irrigated and rainfed fields based on test data. (A) Linear regression, (B) Support vector machine regression (SVM), (C) Random forest (RF) regression, and (D) Deep learning H2O-3.

imagery and advanced ML data analytics for efficient phenotyping. However, it is imperative to recognize possible limitations inherent in the methodologies employed. Such as spatial and spectral resolution of sensors can impact the accuracy and detail of the information. The coverage area and flight altitude may introduce variations in data collection for comparability of results across different flights or study sites. The effectiveness of ML models relies on the quality and quantity of input data, as well as selection of appropriate model architectures and parameters. Biases or errors in the training dataset, as well as overfitting or underfitting of the models, can compromise the accuracy and reliability of predictions. Furthermore, the integration of these technologies introduces practical challenges, such as the need for specialized expertise in data acquisition, processing, and analysis. Constraints related to data availability, computational resources, and software compatibility may also pose challenges on the scalability and accessibility of the methodologies employed.

In future studies, hyperspectral imaging for wheat phenotyping could significantly enhance our capacity to discern nuanced physiological responses and detect subtle indicators of stress within wheat population. Hyperspectral imaging, with broader spectrum of wavelengths and finer resolution, holds promise for unveiling intricate biochemical and biophysical signatures and underlying physiological mechanisms in crops resilience to environmental stresses. Thereby enabling precise predictions of crop behavior and facilitating the development of targeted breeding strategies for improved yield and drought tolerance.

## 5. Conclusion

In conclusion, this study aimed to enhance the digital phenotyping efficiency and reliability to screen wheat genotypes under water limiting condition. This was achieved by UAV multispectral imagery combined with advanced ML algorithms. The results demonstrated the potential of

this integrated approach to effectively assess large population of wheat genotypes under water stress conditions.

The UAV multispectral derived data effectively estimated plant height in this study. The computation of VIs derived from UAV multispectral data provided valuable insights into the physiological responses of wheat genotypes to water stress. NDVI and NDRE exhibited similar trends, with higher values in the IRR experiment, indicating healthier vegetation. The genotype ranking based on yield and stress indices effectively ranked and differentiated wheat genotypes for water stress tolerance and susceptibility. The utilization of ML and DL algorithms for yield prediction proved effective, among four different regression models, DL based H2O-3 model had highest prediction accuracy to estimate yield in wheat genotypes. Similar approaches of low-cost multispectral imagery combined with DL models can be effectively deployed in breeding programs for developing wheat varieties tolerant to drought stress.

## CRediT authorship contribution statement

**Vikas Sharma:** Writing – original draft, Validation, Software, Methodology, Investigation, Formal analysis, Data curation. **Eija Honkavaara:** Writing – review & editing, Validation, Formal analysis. **Matthew Hayden:** Writing – review & editing, Funding acquisition. **Surya Kant:** Writing – review & editing, Supervision, Resources, Project administration, Investigation, Funding acquisition, Conceptualization.

## Declaration of competing interest

The authors declare that they have no known competing financial interests or personal relationships that could have appeared to influence the work reported in this paper.

## Data availability

Data will be made available on request.

## Acknowledgment

We thank all the staff for providing help and support in conducting field experiments.

## Supplementary materials

Supplementary material associated with this article can be found, in the online version, at [doi:10.1016/j.stress.2024.100464](https://doi.org/10.1016/j.stress.2024.100464).

## References

- Aasen, H., Honkavaara, E., Lucieer, A., Zarco-Tejada, P.J., 2018. Quantitative remote sensing at ultra-high resolution with uav spectroscopy: a review of sensor technology, measurement procedures, and data correction workflows. *Remote Sens.* 10, 1091.
- Akram, S., Arif, M.A.R., Hameed, A., 2021. A GBS-based GWAS analysis of adaptability and yield traits in bread wheat (*Triticum aestivum* L.). *J. Appl. Genet.* 62 (1), 27–41. <https://doi.org/10.1007/s13353-020-00593-1>.
- Alotaibi, M., El-Hendawy, S., Mohammed, N., Alsaad, B., Refay, Y., 2023. Appropriate application methods for salicylic acid and plant nutrients combinations to promote morpho-physiological traits, production, and water use efficiency of wheat under normal and deficit irrigation in an arid climate. *Plants* 12 (6), 1368. <https://www.mdpi.com/2223-7747/12/6/1368>.
- Arno Candel, E.L., 2020. Deep Learning with H2O, 6. H2O.ai, Inc., 2307 Leghorn St., Mountain view, CA, 94043. <https://h2o-release.s3.amazonaws.com/h2o/rel-zerme-lo/1/docs-website/h2o-docs/booklets/DeepLearningBooklet.pdf>, 2016.
- Banerjee, B.P., Sharma, V., Spangenberg, G., Kant, S., 2021. Machine learning regression analysis for estimation of crop emergence using multispectral UAV imagery. *Remote Sens. (Basel)* 13 (15), 2918. <https://www.mdpi.com/2072-4292/13/15/2918>.
- Banerjee, B.P., Spangenberg, G., Kant, S., 2020. Fusion of spectral and structural information from aerial images for improved biomass estimation. *Remote Sens. (Basel)* 12 (19), 3164. <https://www.mdpi.com/2072-4292/12/19/3164>.
- Bapela, T., Shimmelis, H., Tsilo, T.J., Mathew, I., 2022. Genetic improvement of wheat for drought tolerance: progress, challenges and opportunities. *Plants (Basel)* 11 (10). <https://doi.org/10.3390/plants11101331>.
- Breiman, L., 2001. Random Forests. *Mach. Learn.* 45 (1), 5–32. <https://doi.org/10.1023/A:1010933404324>.
- Cheng, E., Zhang, B., Peng, D., Zhong, L., Yu, L., Liu, Y., Xiao, C., Li, C., Li, X., Chen, Y., Ye, H., Wang, H., Yu, R., Hu, J., Yang, S., 2022. Wheat yield estimation using remote sensing data based on machine learning approaches [Original Research]. *Front. Plant Sci.* 13 <https://doi.org/10.3389/fpls.2022.1090970>.
- Choudhury, B., Webster, R., Sharma, V., Goswami, J., Meetei, T., Krishnappa, R., Raju, P. L., 2019. Frost damage to maize in northeast India: assessment and estimated loss of yield by hyperspectral proximal remote sensing. *J. Appl. Remote Sens.* 13 (4), 044527 <https://doi.org/10.1111/JRS.13.044527>.
- Chouhan, A., Sur, A., Chutia, D., 2022. DRMNet: difference image reconstruction enhanced multiresolution network for optical change detection. *IEEJ J. Sel. Top. Appl. Earth Obs. Remote Sens.* 15, 4014–4026. <https://doi.org/10.1109/JSTARS.2022.3174780>.
- Chutia, D., Bhattacharyya, D.K., Sarma, J., Raju, P.N.L., 2017. An effective ensemble classification framework using random forests and a correlation based feature selection technique. *Trans. GIS* 21 (6), 1165–1178. <https://doi.org/10.1111/tgis.12268>.
- Clarke, G.N., Hornbrook, M., Lynch, F., Polen, M., Gale, J., Beardslee, W., O'Connor, E., Seeley, J., 2001. A randomized trial of a group cognitive intervention for preventing depression in adolescent offspring of depressed parents. *Arch. Gen. Psychiatry* 58 (12), 1127–1134. <https://doi.org/10.1001/archpsyc.58.12.1127>.
- Córcoles, J.I., Ortega, J.F., Hernández, D., Moreno, M.A., 2013. Estimation of leaf area index in onion (*Allium cepa* L.) using an unmanned aerial vehicle. *Biosyst. Eng.* 115 (1), 31–42. <https://doi.org/10.1016/j.biosystemseng.2013.02.002>.
- Cortes, C., Vapnik, V., 1995. Support-vector networks. *Mach. Learn.* 20 (3), 273–297. <https://doi.org/10.1007/BF00994018>.
- Dang, C., Liu, Y., Yue, H., Qian, J., Zhu, R., 2021. Autumn crop yield prediction using data-driven approaches: support vector machines, random forest, and deep neural network methods. *Can. J. Remote Sens.* 47 (2), 162–181. <https://doi.org/10.1080/07038992.2020.1833186>.
- Gavuzzi, P., Rizza, F., Palumbo, M., Campanile, R.G., Ricciardi, G.L., Borghi, B., 1997. Evaluation of field and laboratory predictors of drought and heat tolerance in winter cereals. *Can. J. Plant Sci.* 77 (4), 523–531. <https://doi.org/10.4141/p96-130>.
- Goswami, J., Sharma, V., Chaudhury, B.U., Raju, P.L.N., 2019. Rapid identification of abiotic stress (frost) in in-field maize crop using UAV remote sensing. *Int. Arch. Photogramm. Remote Sens. Spatial Inf. Sci.* XLII-3/W6, 467–471. <https://doi.org/10.5194/isprs-archives-XLII-3-W6-467-2019>.
- Hafez, E.M., Kheir, A.M.S., Badawy, S.A., Rashwan, E., Farig, M., Osman, H.S., 2020. Differences in physiological and biochemical attributes of wheat in response to single and combined salicylic acid and biochar subjected to limited water irrigation in saline sodic soil. *Plants* 9 (10), 1346. <https://www.mdpi.com/2223-7747/9/10/1346>.
- Ihsan, M.Z., El-Nakhlawy, F.S., Ismail, S.M., Fahad, S., daur, I., 2016. Wheat phenological development and growth studies as affected by drought and late season high temperature stress under arid environment [Original Research]. *Front. Plant Sci.* 7 <https://doi.org/10.3389/fpls.2016.00795>.
- Joshi, A., Pradhan, B., Gite, S., Chakraborty, S., 2023. Remote-sensing data and deep-learning techniques in crop mapping and yield prediction: a systematic review. *Remote Sens. (Basel)* 15 (8), 2014. <https://www.mdpi.com/2072-4292/15/8/2014>.
- Joshi, S., Thoday-Kennedy, E., Daetwyler, H.D., Hayden, M., Spangenberg, G., Kant, S., 2021. High-throughput phenotyping to dissect genotypic differences in safflower for drought tolerance. *PLoS. One* 16 (7), e0254908. <https://doi.org/10.1371/journal.pone.0254908>.
- Koh, J.C.O., Spangenberg, G., Kant, S., 2021. Automated machine learning for high-throughput image-based plant phenotyping. *Remote Sens. (Basel)* 13 (5), 858. <https://www.mdpi.com/2072-4292/13/5/858>.
- LeCun, Y., Bengio, Y., Hinton, G., 2015. Deep learning. *Nature* 521 (7553), 436–444. <https://doi.org/10.1038/nature14539>.
- Li, Y., Li, H., Li, Y., Zhang, S., 2017. Improving water-use efficiency by decreasing stomatal conductance and transpiration rate to maintain higher ear photosynthetic rate in drought-resistant wheat. *Crop J.* 5 (3), 231–239. <https://doi.org/10.1016/j.cj.2017.01.001>.
- Liao, Z.Q., Dai, Y.L., Wang, H., Ketterings, Q.M., Lu, J.S., Zhang, F.C., Li, Z.J., Fan, J.L., 2023. A double-layer model for improving the estimation of wheat canopy nitrogen content from unmanned aerial vehicle multispectral imagery. *J. Integr. Agric.* 22 (7), 2248–2270. <https://doi.org/10.1016/j.jjia.2023.02.022>.
- Liu, X., Liu, W., Tang, Q., Liu, B., Wada, Y., Yang, H., 2022. Global agricultural water scarcity assessment incorporating blue and green water availability under future climate change. *Earth's Future* 10 (4), e2021EF002567. <https://doi.org/10.1029/2021EF002567>.
- Muhammad, F., Raza, M.A.S., Iqbal, R., Zulfiqar, F., Aslam, M.U., Yong, J.W.H., Altaf, M. A., Zulfiqar, B., Amin, J., Ibrahim, M.A., 2022. Ameliorating drought effects in wheat using an exclusive or Co-applied Rhizobacteria and ZnO nanoparticles. *Biology (Basel)* 11 (11), 1564. <https://www.mdpi.com/2079-7737/11/11/1564>.
- Mwinuka, P.R., Mourice, S.K., Mbungu, W.B., Mbilinyi, B.P., Tumbo, S.D., Schmitter, P., 2022. UAV-based multispectral vegetation indices for assessing the interactive effects of water and nitrogen in irrigated horticultural crops production under tropical sub-humid conditions: a case of African eggplant. *Agric. Water. Manage.* 266, 107516. <https://doi.org/10.1016/j.agwat.2022.107516>.
- Naghdyzadegan, J.M., Zand-Parsa, Shahrokh, Razaghi, Fatemeh, Jamshidi, Sajad, Didari, Shohreh, Doosthosseini, Ali, Pourghasemi, Hamid, R., 2023. Developing machine learning models for wheat yield prediction using ground-based data, satellite-based actual evapotranspiration and vegetation indices. *Eur. J. Agronomy* 146, 126820. <https://doi.org/10.1016/j.eja.2023.126820>.
- Panda, S.S., Ames, D.P., Panigrahi, S., 2010. Application of vegetation indices for agricultural crop yield prediction using neural network techniques. *Remote Sens. (Basel)* 2 (3), 673–696. <https://www.mdpi.com/2072-4292/2/3/673>.
- Perry, E.M., Fitzgerald, G.J., Nuttall, J.G., O'Leary, G.J., Schulthess, U., Whitlock, A., 2012. Rapid estimation of canopy nitrogen of cereal crops at paddock scale using a Canopy Chlorophyll Content Index. *Field Crops Res.* 134, 158–164. <https://doi.org/10.1016/j.fcr.2012.06.003>.
- Pimentel, A.J.B., Rocha, J.R.D.A.S.D.C., Souza, M.A.d., Ribeiro, G., Silva, C.R., Oliveira, I. C.M., 2015. Characterization of heat tolerance in wheat cultivars and effects on production components. *Revista Ceres* 62.
- Pinto, F., Zaman-Allah, M., Reynolds, M., Schulthess, U., 2023. Satellite imagery for high-throughput phenotyping in breeding plots [Perspective]. *Front. Plant Sci.* 14 <https://doi.org/10.3389/fpls.2023.1114670>.
- Qiao, L., Tang, W., Gao, D., Zhao, R., An, L., Li, M., Sun, H., Song, D., 2022. UAV-based chlorophyll content estimation by evaluating vegetation index responses under different crop coverages. *Comput. Electron. Agric.* 196, 106775 <https://doi.org/10.1016/j.compag.2022.106775>.
- Qiao, M., He, X., Cheng, X., Li, P., Luo, H., Zhang, L., Tian, Z., 2021. Crop yield prediction from multi-spectral, multi-temporal remotely sensed imagery using recurrent 3D convolutional neural networks. *Int. J. Appl. Earth Observ. Geoinf.* 102, 102436 <https://doi.org/10.1016/j.jag.2021.102436>.
- Roselle, A.A., Hamblin, J., 1981. Theoretical aspects of selection for yield in stress and non-stress environments. *Crop Sci.* 21 (6) <https://doi.org/10.2135/cropsci1981.0011183X02100060033x>.
- Rouse, J.W., 1973. Monitoring vegetation systems in the great plains with ERTS. In: Third ERTS Symposium, 1. NASA, Washington, DC, pp. 309–317. 1973. <https://cir.nii.ac.jp/crid/1573105975083785728>.
- Ruan, G., Li, X., Yuan, F., Cammarano, D., Ata-Ul-Karim, S.T., Liu, X., Tian, Y., Zhu, Y., Cao, W., Cao, Q., 2022. Improving wheat yield prediction integrating proximal sensing and weather data with machine learning. *Comput. Electron. Agric.* 195, 106852 <https://doi.org/10.1016/j.compag.2022.106852>.
- Salem, E.M.M., Kenawey, M.K.M., Saudy, H.S., Mubarak, M., 2022. Influence of silicon forms on nutrients accumulation and grain yield of wheat under water deficit conditions. *Gesunde Pflanzen* 74 (3), 539–548. <https://doi.org/10.1007/s10343-022-00629-y>.
- Sankaran, S., Khot, L.R., Carter, A.H., 2015. Field-based crop phenotyping: multispectral aerial imaging for evaluation of winter wheat emergence and spring stand. *Comput. Electron. Agric.* 118, 372–379. <https://doi.org/10.1016/j.compag.2015.09.001>.
- Sankaran, S., Zhou, J., Khot, L.R., Trapp, J.J., Mndolwa, E., Miklas, P.N., 2018. High-throughput field phenotyping in dry bean using small unmanned aerial vehicle based

- multispectral imagery. *Comput. Electron. Agric.* 151, 84–92. <https://doi.org/10.1016/j.compag.2018.05.034>.
- Schneider, A., Hommel, G., Blettner, M., 2010. Linear regression analysis: part 14 of a series on evaluation of scientific publications. *Dtsch. Arztebl. Int.* 107 (44), 776–782. <https://doi.org/10.3238/arztebl.2010.0776>.
- Sharma, V., Baruah, D., Chutia, D., Raju, P., Bhattacharya, D.K., 2016. An assessment of support vector machine kernel parameters using remotely sensed satellite data. In: 2016 IEEE International Conference on Recent Trends in Electronics, Information & Communication Technology (RTEICT).
- Shiferaw, B., Smale, M., Braun, H.-J., Duveiller, E., Reynolds, M., Muricho, G., 2013. Crops that feed the world 10. Past successes and future challenges to the role played by wheat in global food security. *Food Secur.* 5 (3), 291–317. <https://doi.org/10.1007/s12571-013-0263-y>.
- Srivastava, A.K., Safaei, N., Khaki, S., Lopez, G., Zeng, W., Ewert, F., Gaiser, T., Rahimi, J., 2022. Winter wheat yield prediction using convolutional neural networks from environmental and phenological data. *Sci. Rep.* 12 (1), 3215. <https://doi.org/10.1038/s41598-022-06249-w>.
- Su, J., Liu, C., Coombes, M., Hu, X., Wang, C., Xu, X., Li, Q., Guo, L., Chen, W.-H., 2018. Wheat yellow rust monitoring by learning from multispectral UAV aerial imagery. *Comput. Electron. Agric.* 155, 157–166. <https://doi.org/10.1016/j.compag.2018.10.017>.
- Tang, Q., 2020. Global change hydrology: terrestrial water cycle and global change. *Sci. China Earth. Sci.* 63 (3), 459–462. <https://doi.org/10.1007/s11430-019-9559-9>.
- Tattaris, M., Reynolds, M.P., Chapman, S.C., 2016. A direct comparison of remote sensing approaches for high-throughput phenotyping in plant breeding [Original Research]. *Front. Plant Sci.* 7 <https://doi.org/10.3389/fpls.2016.01131>.
- Thoday-Kennedy, E., Banerjee, B., Panizzo, J., Maharjan, P., Hudson, D., Spangenberg, G., Hayden, M., Kant, S., 2023. Dissecting physiological and agronomic diversity in safflower populations using proximal phenotyping. *Agriculture* 13 (3), 620. <https://www.mdpi.com/2077-0472/13/3/620>.
- Wilke, N., Siegmann, B., Postma, J.A., Muller, O., Krieger, V., Pude, R., Rascher, U., 2021. Assessment of plant density for barley and wheat using UAV multispectral imagery for high-throughput field phenotyping. *Comput. Electron. Agric.* 189, 106380 <https://doi.org/10.1016/j.compag.2021.106380>.
- Wolters, S., Söderström, M., Piikki, K., Börjesson, T., Pettersson, C.-G., 2022. Predicting grain protein concentration in winter wheat (*Triticum aestivum* L.) based on unpiloted aerial vehicle multispectral optical remote sensing. *Acta Agriculturae Scandinavica, Section B — Soil Plant Sci.* 72 (1), 788–802. <https://doi.org/10.1080/09064710.2022.2085165>.
- Xie, T., Li, J., Yang, C., Jiang, Z., Chen, Y., Guo, L., Zhang, J., 2021. Crop height estimation based on UAV images: methods, errors, and strategies. *Comput. Electron. Agric.* 185, 106155 <https://doi.org/10.1016/j.compag.2021.106155>.
- Yan, W., Zhong, Y., Shangguan, Z., 2016. A meta-analysis of leaf gas exchange and water status responses to drought. *Sci. Rep.* 6 (1), 20917. <https://doi.org/10.1038/srep20917>.
- Zarea, M.J., Karimi, N., 2023. Grain yield and quality of wheat are improved through post-flowering foliar application of zinc and 6- benzylaminopurine under water deficit condition [Original Research]. *Front. Plant Sci.* 13 <https://doi.org/10.3389/fpls.2022.1068649>.
- Zhou, X., Kono, Y., Win, A., Matsui, T., Tanaka, T.S.T., 2021a. Predicting within-field variability in grain yield and protein content of winter wheat using UAV-based multispectral imagery and machine learning approaches. *Plant Prod. Sci.* 24 (2), 137–151. <https://doi.org/10.1080/1343943X.2020.1819165>.
- Zhou, Y., Lao, C., Yang, Y., Zhang, Z., Chen, H., Chen, Y., Chen, J., Ning, J., Yang, N., 2021b. Diagnosis of winter-wheat water stress based on UAV-borne multispectral image texture and vegetation indices. *Agric. Water. Manage.* 256, 107076. <https://doi.org/10.1016/j.agwat.2021.107076>.